



Asymmetric spinning for offset blanks

Yong Xiao^{1,2} · Zhiren Han^{1,2} · Shuyang Zhou^{1,2} · Zhen Jia²

Received: 10 October 2019 / Accepted: 23 February 2020 / Published online: 20 March 2020
© Springer-Verlag London Ltd., part of Springer Nature 2020

Abstract

Various approaches have been attempted by researchers to break through the limitation of axisymmetric shape in metal spinning. In this study, a synchronous multipass spinning method for offset blanks is proposed. The motion of the roller and the rotation of the mandrel are synchronized to achieve asymmetric shapes. The roller trajectory is represented by a set of scattered data which contains the axial position of the roller, the radial position of the roller, and the rotational angle of the mandrel. Conventional spinning for offset blanks is also conducted in comparison with synchronous spinning. The geometries of the products with different offset values λ are examined. The axial distribution of wall thickness varies at different circumferential positions of the product due to the oblique shape. The thickness increases from the short side to the long side of the product. A larger offset value λ results in a larger product diameter due to the springback of the material. Forming limits in terms of roller feed ratio f , offset value λ , blank thickness t_0 , blank diameter D , and the number of passes are investigated. Both fracture and wrinkling occur in the experiments. Due to the oblique shape, wrinkling tends to occur during the first several passes on the long side of the flange, and fracture tends to occur during the last several passes on the long side of the product. The experiments are more likely to succeed when a small offset ratio λ , a small blank diameter D , a small feed ratio f , or a large blank thickness t_0 is used. Compared with synchronous spinning, the difference between the axial thickness distributions on both sides of the product is smaller in conventional spinning due to the uniform feed ratio. In terms of forming limits, conventional spinning has a slightly better performance.

Keywords Metal spinning · Offset blanks · Asymmetric multipass spinning · Forming limit

1 Introduction

Metal spinning usually refers to a metal forming process where a flat sheet metal blank is formed into an axisymmetric hollow shape by a roller which gradually forces the blank onto a mandrel. The technology is widely used in automotive and aerospace industries for producing axisymmetric sheet metal components. It has many advantages when compared with conventional press forming. The deformation of the material is localized. The intensity of the roller pressure is higher than

the press forming process. Thus, it requires low-forming forces for the high-strength material. It can also improve both the surface quality and the mechanical strength of the parts.

For traditional spinning techniques, the classification into conventional spinning, shear spinning, and tube spinning is widely accepted [1]. In order to break through the limitation of producing axisymmetric shapes, many approaches have been developed to achieve asymmetric shapes in metal spinning. They are roughly categorized into three types: using a dedicated mechanism; force-controlled spinning; and synchronous spinning.

The first attempt on asymmetric spinning was using cams and links. Amano and Tamura [2] used an offset roller to form elliptical shapes in shear spinning. This method had difficulty to achieve desired roller-mandrel clearance and resulted in weak accuracy. Gao et al. [3] investigated the forming of elliptical parts in conventional spinning and shear spinning using an offset mandrel. The results showed that the dimensional accuracy of the produced parts in conventional spinning is high, and the thickness distribution in shear spinning agrees

✉ Zhiren Han
hanren888@163.com

¹ School of Mechanical Engineering, Northwestern Polytechnical University, Shannxi 710072, China

² Key Lab of Fundamental Science for National Defense of Aeronautical Digital Manufacturing Process, Shenyang Aerospace University, Shenyang 110136, China

with the sine law. Xia et al. [4] developed a spinning machine in which the axis of the mandrel can be translated and tilted for each pass of the roller to achieve eccentric or oblique tube shapes. The mechanism of non-axisymmetric tube spinning is investigated through numerical simulation and experiments [5, 6]. Xia et al. [7] developed the profiling driving spinning method which enables the formation of non-circular hollow cone shapes. A pair of gears is used to synchronize the radial movement of the roller and the rotation of the mandrel.

In force-controlled spinning, the pushing force of the roller is controlled to push the material onto the mandrel. Awiszus and Meyer [8] produce non-circular shapes using spring-controlled rollers on a standard spinning machine. The thickness distribution cannot be controlled. The authors suggested that numerically controlled rollers would have better performance. A hybrid position/force control system is applied to form non-axisymmetric shapes by Arai [9]. The roller tracks the non-axisymmetric mandrel under the regulated pushing force. Arai [10] designed a novel spinning machine in which the roller is driven by linear motors. The forming time performance was improved.

In synchronous spinning, the motion of the roller and the rotation of the mandrel are synchronized. This method can achieve non-circular or oblique shapes with or without a mandrel. Shimizu [11] developed a pulse-controlled synchronous spinning machine to achieve asymmetric shapes. The shapes of the products, strain distributions, and force components were investigated. Han et al. [12] developed a synchronous spinning method in a CNC (computerized numerical controlled) spinning machine. The tool path for eccentric cones was deduced through the mathematical method. The mechanism of the forming process is also studied through numerical simulation [13]. This method can be easily altered to form non-circular shapes. Jia et al. [14, 15] adapted this method to achieve squared-cone products; the mechanism of the forming process was investigated using finite element analysis. Härtel and Laue [16] used a preformed conical to optimize the non-circular spinning process. The optimization based on the numerical simulation showed that the sheet thinning could be reduced by nearly 30%. Sekiguchi and Arai [17] developed an oblique spinning method to control the thickness distribution in mandrel-free shear spinning. The synchronous spinning method results in radial displacement of the flange in the final product. The author suggested that material wastage can be suppressed by offsetting the radial position of the blank. Han et al. [18] applied the method from Sekiguchi and Arai [17] on oblique cones to achieve uniform thickness distribution.

These methods above are similar to traditional shear spinning. The process contains one roller pass, and perpendicular walls cannot be achieved since the wall thickness would be zero based on the sine law. Therefore, synchronous multipass spinning methods were developed to achieve vertical walls. The box shapes with vertical walls were successfully formed

in multipass synchronous spinning by Sugita and Arai [19]. The parameters and the forming limit using two kinds of pass sets were investigated. Arai and Kanazawa [20] proposed a synchronous spinning method which enables the formation of circular and squared cups with oblique bottoms. The roller is controlled axially within one rotation of the mandrel to achieve oblique shapes. The non-uniform wall thickness distribution is optimized by using an intermediate shape. Xiao et al. [21] developed an asymmetric multipass spinning method for angled flange cylinders. The wall thickness distribution is non-uniform, and the length of the flange varies circumferentially due to the inclination.

Normally, the blanks are placed in the center of the mandrel in the process. With the development of synchronous spinning, many of the products have oblique shapes, in which the lengths of the walls or the flanges vary circumferentially. Offset blanks can reduce material wastage in a way. This paper deals with cylindrical cups in multipass spinning with offset blanks. Both synchronous spinning and conventional spinning are used to investigate how the spinning method affects the final product. Section 2 describes the calculation of the roller trajectory in synchronous spinning. Section 3 describes the experiment setup. Section 4 discusses the effect of parameters on product geometry. Section 5 shows the result of the forming limit. Section 6 summarizes the main conclusions of this study.

2 Methodology

2.1 Offset blank spinning

The blanks in the experiment are clamped between mandrel and tailstock with a radially offset value L as shown in Fig. 1.

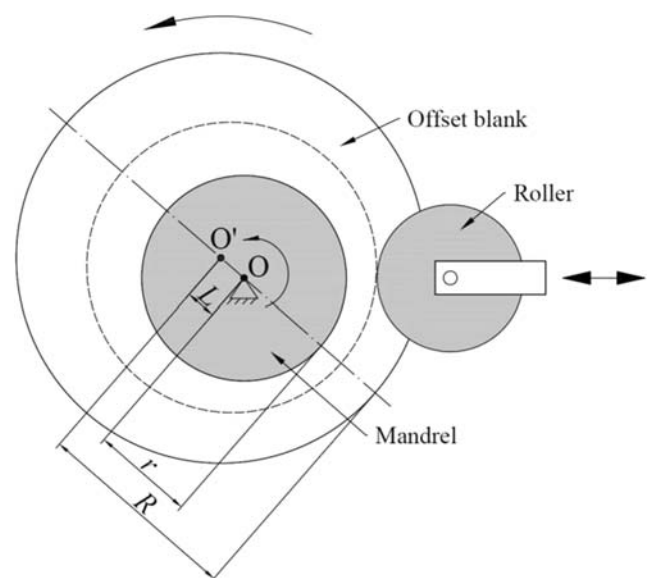


Fig. 1 Setup of asymmetric spinning for offset blanks

The offset ratio is defined as $\lambda = L/(R-r)$. R is the radius of the blank, and r is the radius of the mandrel. The blank is placed in the center of the mandrel when $\lambda = 0$; the edge of the blank reaches the edge of the mandrel when $\lambda = 1$.

The shape can be formed in both conventional spinning and synchronous spinning. Figure 2 shows the roller trajectory during one of the passes with an offset blank. In this paper, “trajectory” means the contact lines on the product between the roller and the blank during spinning; “pass” means the roller’s motion in its two-dimensional plane. The product shape during each pass is considered as an oblique curved cone shape which is cut from a curved cone shape that has circular cross sections.

Roller feed ratio f is defined as the distance of the roller’s movement in one rotation of the spindle. In conventional spinning, the roller trajectory is a spiral line. The feed ratio stays constant, and the roller moves along the roller pass either away from the mandrel (in a forward pass) or toward it (in a backward pass). However, due to the oblique edge of the product, the roller may move away and toward the edge (broken lines in Fig. 2) in a single rotation of the mandrel which could cause collision between the roller and the material. In synchronous spinning, the roller trajectory is an oblique spiral shape that stays on the surface of the product. Therefore, collisions could be avoided. The synchronous spinning method can also achieve certain asymmetric shapes which cannot be achieved by the conventional spinning method such as the angled-flange cylinder [21]. However, the roller moves back and forth along the roller pass in every rotation of the mandrel which leads to a non-uniform feed ratio. This may cause an uneven material flow. The effect of these spinning

techniques on the final products will be discussed in Sections 4 and 5.

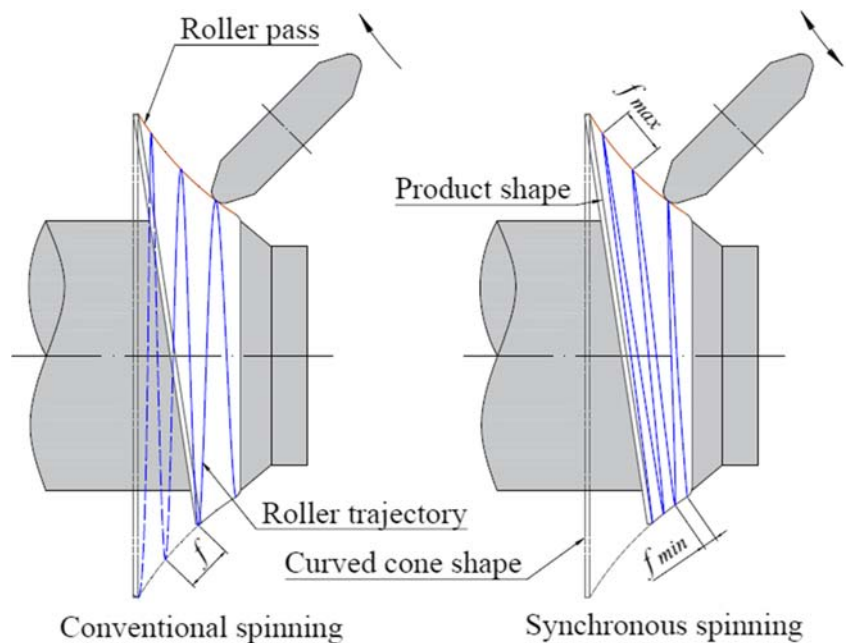
2.2 Roller trajectory for offset blank in synchronous spinning

In conventional spinning, the roller pass is composed of 2D data which contains radial and axial positions of the roller, whereas, in synchronous spinning, the roller pass is represented by 3D data containing radial and axial positions of the roller and the rotational positions of the mandrel. The roller’s movement is calculated based on a pair of pass sets.

2.2.1 Pass set design

The schematic of the pass design is illustrated in Fig. 3. A pair of pass sets is designed in order to calculate the roller trajectory. The pass sets are composed of arc lines. The concavity of the pass γ is expressed as $\gamma = h/L_l$. h is the distance between the midpoint of the pass and the midpoint of $p_s p_e$. L_l is the distance between p_s and p_e . On the long side, the pass rotates around the same start point, and the angle of the end point to the start point for each pass is decreased by $\Delta\alpha$. The end of each pass is approximated by an ellipse whose semimajor axis is OA and passes through point $B (-H, d/2)$. On the short side, the pass set is a cut-mirrored shape of the long side. An ellipse whose semimajor axis is OA' and passes through point $B' (-H', -d/2)$ is used to approximate the end point of each pass. The coordinates of point B and B' are determined through trial and error.

Fig. 2 Roller trajectory during one pass



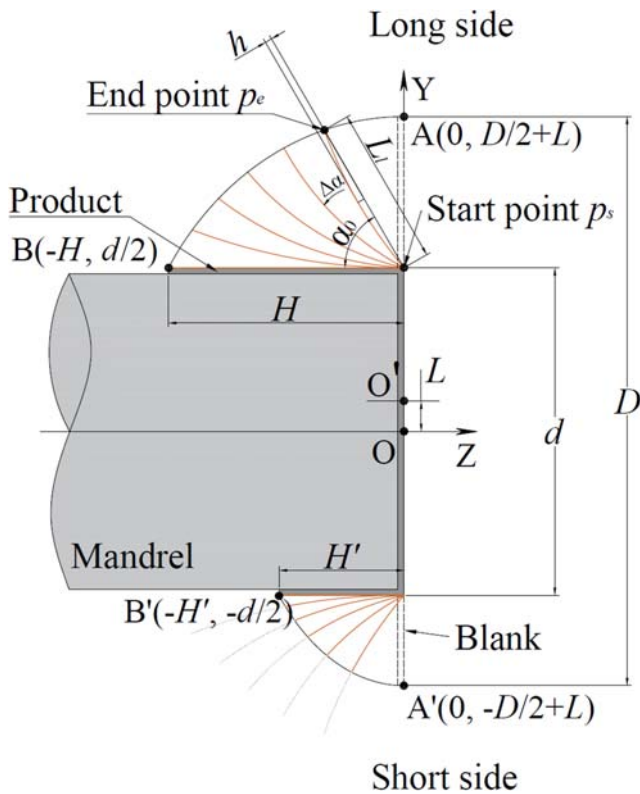
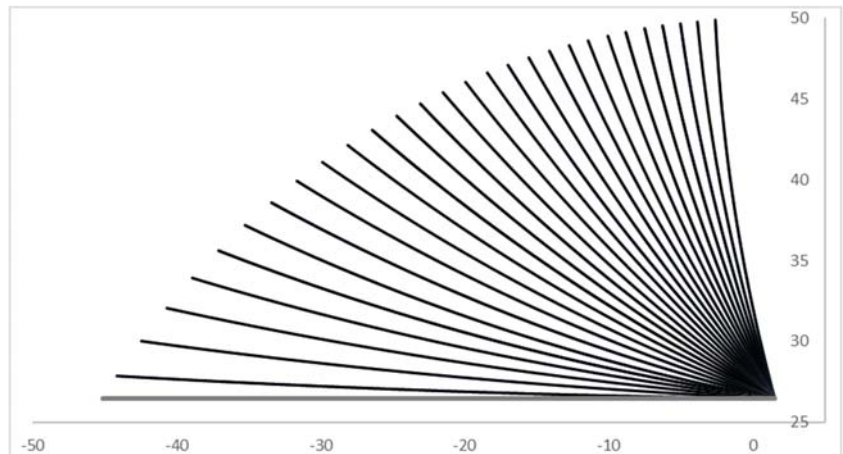


Fig. 3 Design of roller passes for synchronous spinning

Figure 4 shows an example of the pass set. The pass sets used in this study contain 28 or 14 curved lines with $\alpha_0 = 80^\circ$ and $\gamma = 0.03$ (for the last several passes, γ is set to a smaller value to keep the clearance between the roller and the mandrel). A conventional linear pass along the mandrel with a mandrel-roller clearance equals to the blank thickness t_0 and a roller feed ratio of $f = 1$ mm/rev was used to push the material onto the mandrel in all the products.

Fig. 4 An example of a pass set containing 28 curved passes



2.2.2 Calculation of roller trajectory

Figure 5 illustrates the calculation of the roller trajectory of one pass in synchronous spinning. The general roller feed ratio f is used to describe the non-uniform feed ratio. The number of revolutions of the mandrel during one pass n is determined by the following equation:

$$n = \left\lceil \frac{L_s + L_l}{2f} \right\rceil \tag{1}$$

where L_s is the length of the pass on the short side and L_l is the length of the pass on the long side. The roller feed ratio reaches its minimum value f_{\min} ($f_{\min} = L_s/n$) on the short side and reaches the maximum value f_{\max} ($f_{\max} = L_l/n$) on the long side.

The roller's position $T(z, \rho, \theta)$ during one of the passes is described by three variations: the axial position of the roller z , the radial position of the roller ρ , and the rotational position of the mandrel θ .

The passes on both sides are divided into $2n$ line segments. The roller trajectory of the pass is a spiral line ($p_{s,0}, p_{l,1}, p_{s,2}, p_{l,3}, p_{s,4}, \dots, p_{s,2n}$) which starts at point $p_{s,0}$ and ends at point $p_{s,2n}$. The axial position (z -axis) of the roller is expressed as the followed equation:

$$\begin{cases} z(\theta) = z_{s,2i-2} + (z_{l,2i-1} - z_{s,2i-2}) \frac{\theta - (2i-2)\pi}{\pi}, & \theta \in [2(i-1)\pi, (2i-1)\pi) \\ z(\theta) = z_{l,2i-1} + (z_{s,2i} - z_{l,2i-1}) \frac{\theta - (2i-1)\pi}{\pi}, & \theta \in [(2i-1)\pi, 2i\pi) \end{cases} \tag{2}$$

where z_i is the z -coordinate of p_i , z_s is the z -coordinate of $p_{s,0}$, and $i = \lceil \frac{\theta}{2\pi} \rceil$ ($i \in [1, n]$) is the number of the rotations of the mandrel.

The radial position of the roller ρ when the rotational angle is θ can be obtained from the y -coordinate of the upper pass (long side) which is the radius of the cross section $S_z(\theta)$.

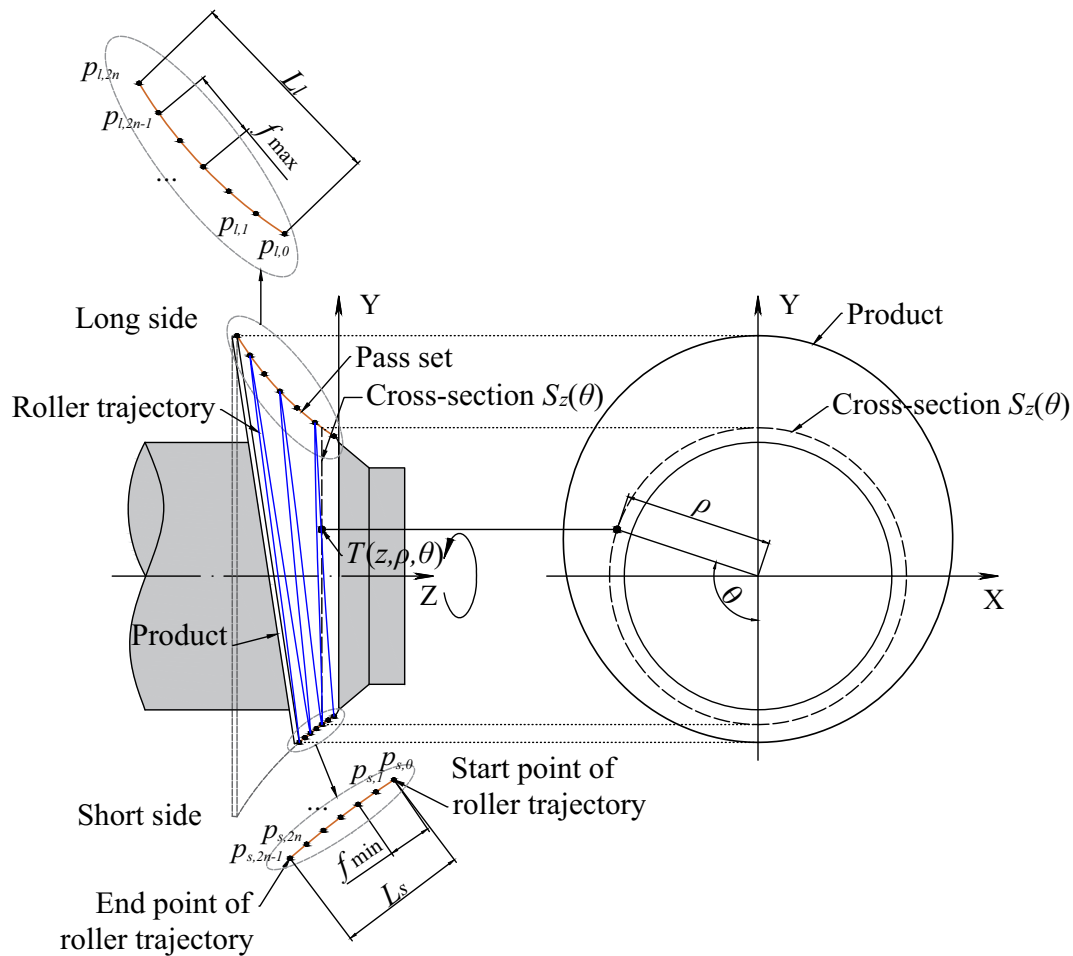


Fig. 5 Calculation of the roller trajectory

At last, the roller trajectory is interpolated into points every 5° of the rotational angle θ as shown in Fig. 6. Solid dots represent the positions of the roller. The circumferential thickness distribution could be unsymmetric in multipass oblique spinning due to the back-and-forth movement of the roller [21]. Therefore, the rotational direction of the mandrel is reversed every pass to suppress the torsion for all the products in the experiment. Due to the non-axisymmetric shape of the roller trajectory, the compensation for the roller radius of the spinning machine cannot be applied in synchronous spinning. For comparison, the product is also formed without compensation in conventional spinning in this paper.

3 Experiment setup

All the experiments are performed on a CNC spinning machine (PS-CNCSXY600-5) as shown in Fig. 7. The spindle is driven by an 11-kW servomotor, and the axial and radial motion of the roller is controlled by two

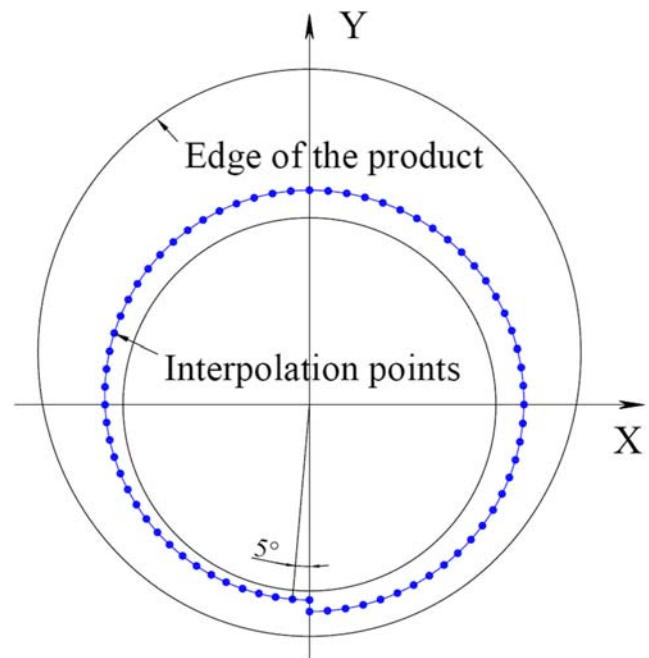


Fig. 6 Interpolation of the roller trajectory

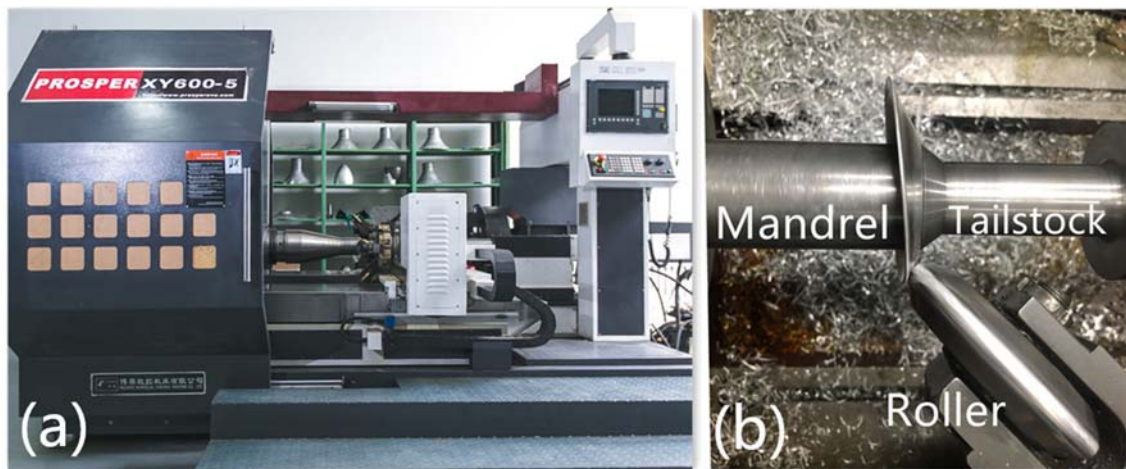


Fig. 7 PS-CNC SXY600-5 NC spinning lathe: **a** full view of the lathe and **b** working portion of spinning

sophisticated servomotors with a positional accuracy of 0.025 mm. The blank is clamped between a mandrel and a tailstock. The tailstock rotates along with the mandrel which is driven by the spindle. The diameter of the roller is 110 mm, and the nose radius is 6 mm. The roller is inclined by 45° to the spindle axis.

Circular disks made of aluminum alloy (6061) with different diameters and thicknesses were used as sheet blanks in this study. The diameter of the cylindrical mandrel is 50 mm. Marks are drawn on the offset blanks with ruler and compass for calibration and leveling as shown in Fig. 8 a. The blank is clamped between mandrel and tailstock; the initial position of the blank is determined using a plumb line by rotating the mandrel, as illustrated in Fig. 8 b. The rotational speed is 30 rpm and 150 rpm in synchronous spinning and conventional spinning, respectively.

The thicknesses of the products were measured using a micrometer with an accuracy of 0.01 mm. The diameters

and the heights of the products were measured using a caliper with an accuracy of 0.02 mm.

4 Product geometry

Experiments of synchronous spinning and conventional spinning are conducted to investigate the effect of offset ratio λ on the product geometry of offset blanks. The parameters are shown in Table 1.

Figure 9 shows a photograph of the formed products. The cylindrical cups have an oblique edge due to the offset blanks. The greater the offset ratio, the larger the inclination angle. The wall thickness distributions and the heights of the products were measured at different circumferential positions. The diameter distributions of the products were measured between 90° and 270° position due to the oblique edge.

Fig. 8 Experiment setup: **a** marks on the blank and **b** determination of the initial position

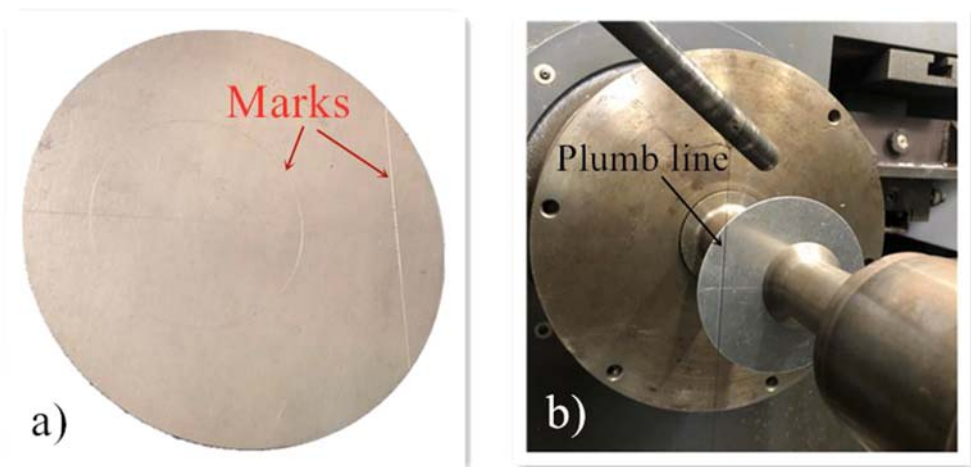


Table 1 Parameters of experiments for product geometry

Roller feed ratio f (mm/rev)	1
Blank diameter D (mm)	100
Offset ratio λ	0, 0.1, 0.2, 0.3, 0.4
Blank thickness t_0 (mm)	1.5
Number of passes	28

4.1 Thickness distribution

Figure 10 shows the axial distributions of thickness ratio at different circumferential positions of the products formed in synchronous spinning with parameters of $\lambda = 0.4$, $D = 100$ mm, and $t_0 = 1.5$ mm. The thickness distributions between the left side (from 0° to 180°) and the right side (from 180° to 360°) of the product are nearly symmetrical due to the reversion of the rotational direction of the spindle. Therefore, only the distributions from 0° to 180° directions are shown in the figures. The dotted line is the thickness ratio when $\lambda = 0$, $D = 100$ mm, and $t_0 = 1.5$ mm. The thickness distributions near the short side (0°) tend to decrease axially, and they are smaller than the original blank thickness t_0 . Whereas the thickness distributions near the long side (180°) are larger than t_0 and they have wave shapes, the axial distribution of thickness ratio at 90° position when $\lambda = 0.4$ is nearly in agreement with that when $\lambda = 0$. A small feed ratio would result in excessive material flow in the outward direction which causes thinning on the product [22]. Therefore, the smaller feed ratio near the short side causes more thinning than that near the long side of the product.

Figure 11 shows the distributions of thickness ratio on the short side (0°) and the long side (180°) when $\lambda = 0, 0.1, 0.2, 0.3$, and 0.4 . The dotted line is the distribution of thickness ratio when $\lambda = 0$. When a larger λ is used, the wall has more thinning on the short side, and it thickens more on the long side. Due to the calculation method of the roller trajectory, a bigger λ would result in smaller f near the short side and larger f near the long side. Therefore, the bigger λ caused larger differences in the thickness ratio distributions of the product.

Figure 12 shows the axial distributions of thickness ratio at different circumferential positions of the product

formed in conventional spinning with parameters of $\lambda = 0.4$, $D = 100$ mm, and $t_0 = 1.5$ mm. The thickness distribution in conventional spinning shares a similar pattern with that in synchronous spinning. Due to the uniform roller feed ratio, the difference between the thickness distributions in conventional spinning is much smaller than that in synchronous spinning.

OA and OA' (from Fig. 3) are the distances from the center of the mandrel to the edge of the blank on the long side (180°) and the short side (0°), respectively. The distribution of the thickness ratio on each side of the product when $\lambda = 0.1, 0.2, 0.3$, and 0.4 is compared with the product when $\lambda = 0$ with a blank radius equals to OA or OA' in conventional spinning as illustrated in Figs. 13, 14, 15, 16. The wall thickness (broken lines) of the product with $\lambda = 0$ is nearly constant when the blank diameter is small, and it has wavy shapes (dotted lines) when a large diameter is used. The distributions of wall thickness ratio on the long side or the short side of the product when $\lambda > 0$ has a similar distribution with the product with a radius equals to OA or OA' when $\lambda = 0$. This suggests that the thickness distributions along different directions in offset blanks could be predicted by the distances from the center of the mandrel to the edge of the blank and the roller feed rate along that direction.

4.2 Product diameter

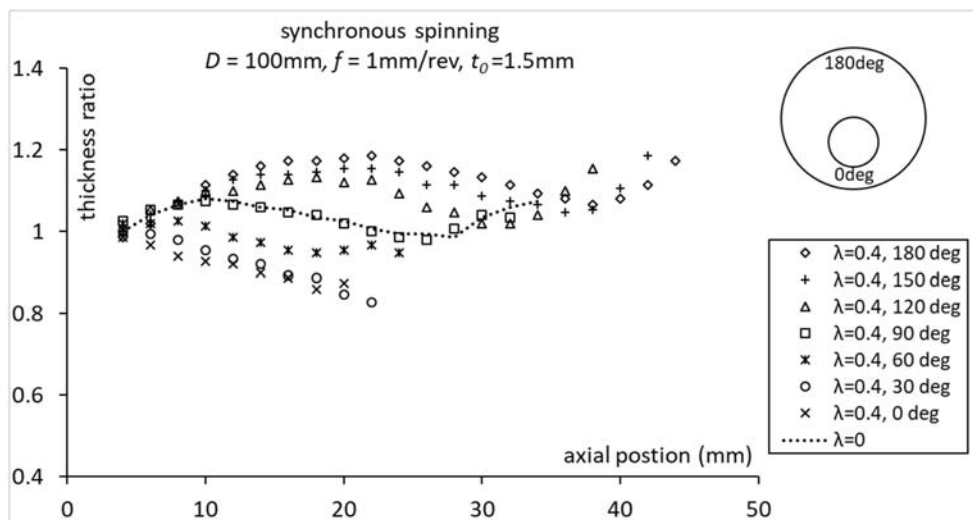
Figure 17 shows the diameters of the products with parameters of $\lambda = 0, 0.1, 0.2, 0.3$, and 0.4 ; $D = 100$ mm; and $t_0 = 1.5$ mm in synchronous spinning. The diameter is larger than the target value (broken line), and it expands toward the edge of the product wall due to the springback of the material. A larger λ means there is less material on the short side to “force” the material on the long side onto the mandrel, which causes larger diameters in general.

Figure 18 shows the diameter distributions of the products with parameters of $\lambda = 0, 0.1, 0.2, 0.3$, and 0.4 ; $D = 100$ mm; and $t_0 = 1.5$ mm in conventional spinning. The diameters near the top of the product formed in conventional spinning are nearly the same with that in synchronous spinning. It expands more toward the edge compared

Fig. 9 Photograph of the products formed in synchronous spinning ($D = 100$ mm, $\lambda = 0.1, 0.2, 0.3, 0.4$ from left to right)



Fig. 10 Axial distributions of wall thickness ratio at different circumferential positions



with synchronous spinning. Springback would increase when a higher feed ratio is used [23]. Due to the calculation of the roller trajectory in synchronous spinning, the roller feed is denser than that in conventional spinning with the same parameter f as shown in Fig. 2. This may cause larger springback in conventional spinning.

4.3 Product height

Figure 19 is the schematic of the height estimation. The shaded regions (from angle θ to angle $\theta + \Delta\theta$, $\Delta\theta \rightarrow 0$.) are used to calculate the height at circumferential position θ . R is the radius of the blank, r is the radius of the mandrel, t_0 is the thickness of the blank, h is the distance from the center of the mandrel to the edge of the blank, and L is the offset value. The theoretical height of the wall was roughly estimated using the following assumptions: (a) the volume of the material remains constant during the process; (b) the average thickness

of the product wall equals the original blank thickness; and (c) the material in region A stays constant as part of the top of the product; the material in region C is forming into the wall with region B as the bottom.

The volume of region ABC is calculated as:

$$V_{ABC} \approx \pi h^2 \frac{\Delta\theta}{2\pi} t_0 \tag{3}$$

The values of h and α can be obtained by sine law:

$$h = R \sin(\theta - \alpha) / \sin \theta \tag{4}$$

$$\alpha = \sin^{-1}(L \sin \theta / R) \tag{5}$$

The volume of region A is calculated as:

$$V_A = \pi r^2 \frac{\Delta\theta}{2\pi} t_0 \tag{6}$$

Fig. 11 Axial distributions of wall thickness ratio on the long side (180°) and the short side (0°) with different λ

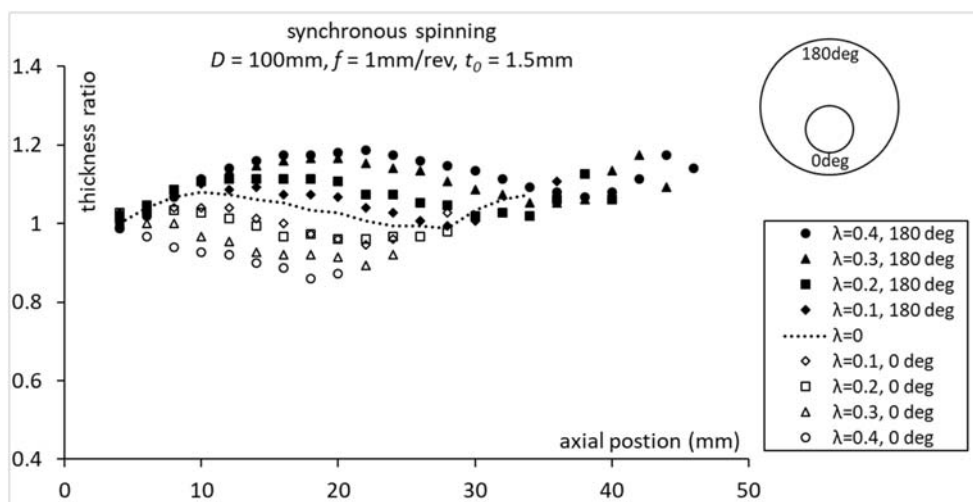


Fig. 12 Axial distributions of wall thickness ratio at different circumferential positions in conventional spinning

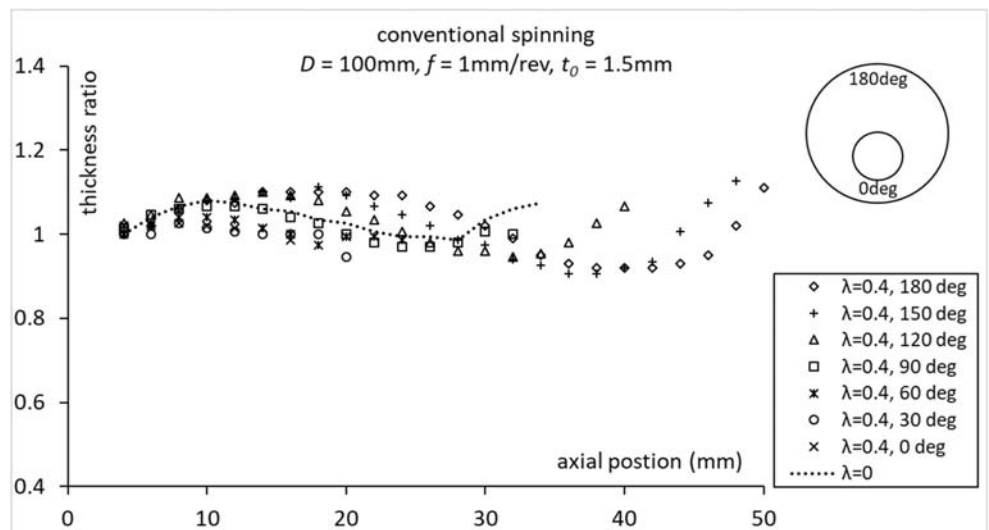


Fig. 13 Comparison of thickness ratio between synchronous spinning ($\lambda = 0.1$) and conventional spinning ($\lambda = 0$)

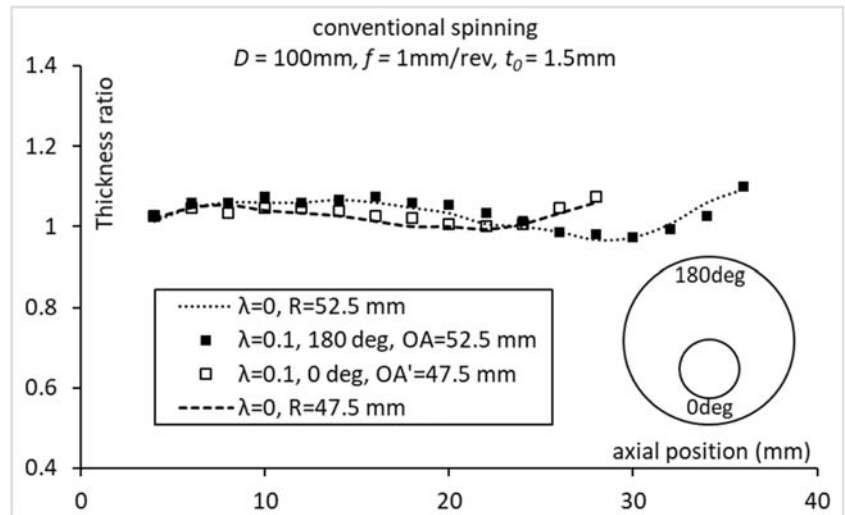


Fig. 14 Comparison of thickness ratio between synchronous spinning ($\lambda = 0.2$) and conventional spinning ($\lambda = 0$)

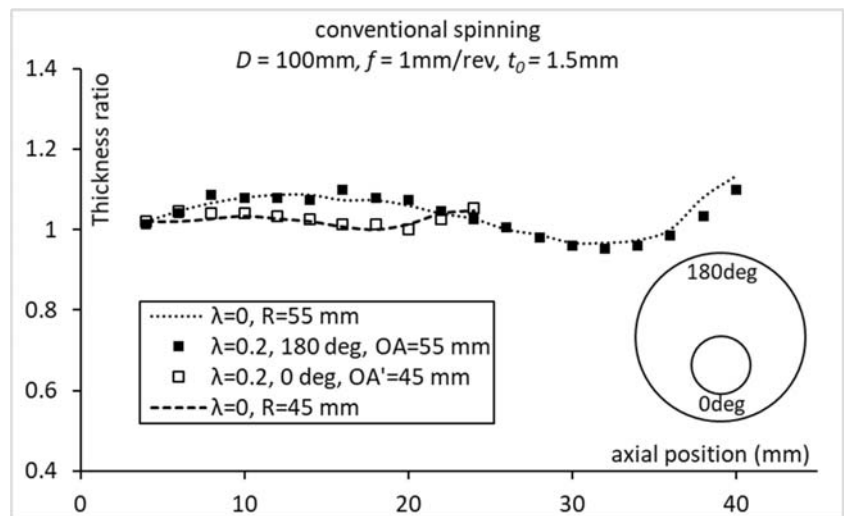


Fig. 15 Comparison of thickness ratio between synchronous spinning ($\lambda = 0.3$) and conventional spinning ($\lambda = 0$)

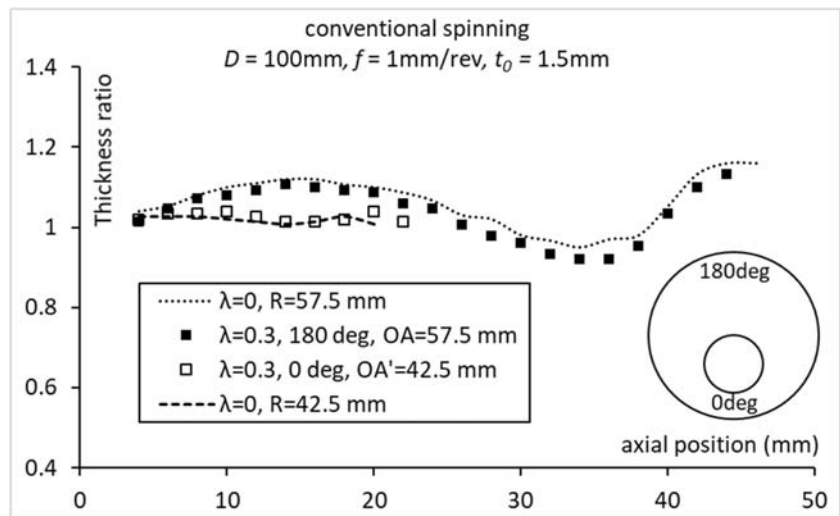


Fig. 16 Comparison of thickness ratio between synchronous spinning ($\lambda = 0.4$) and conventional spinning ($\lambda = 0$)

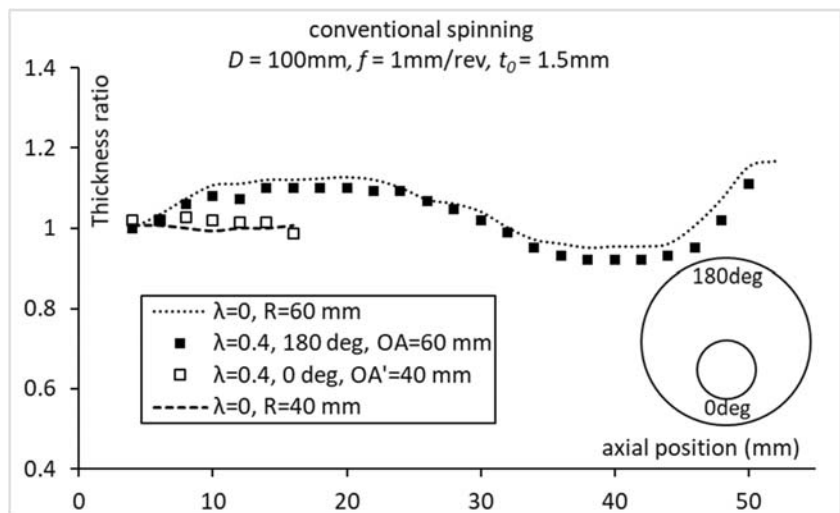


Fig. 17 Distributions of product diameters between 90° and 270° in synchronous spinning

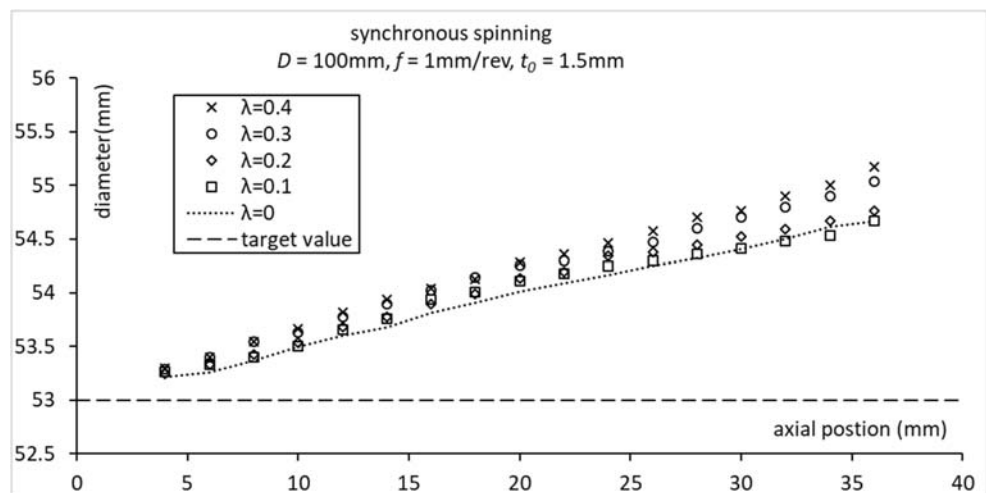
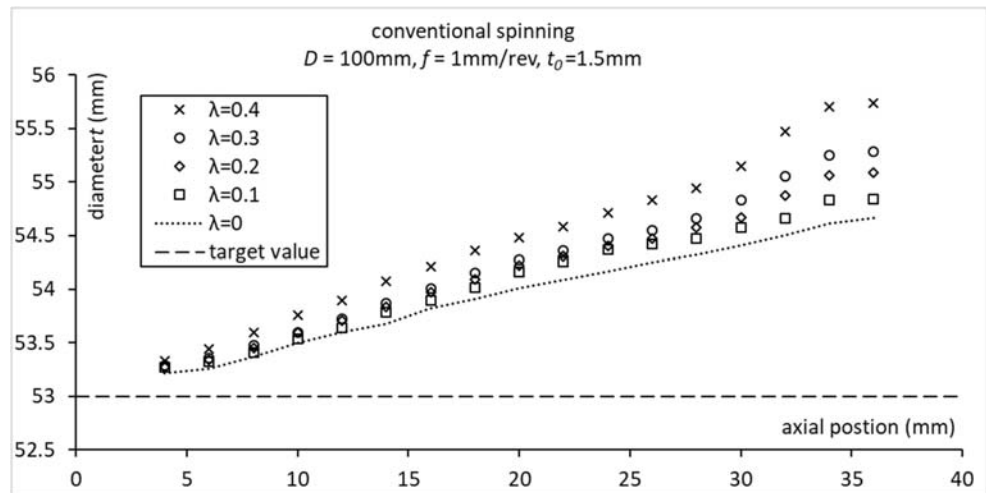


Fig. 18 Distributions of product diameters between 90° and 270° in conventional spinning



The area of region B is:

$$S_B = \pi(r + t_0)^2 \frac{\Delta\theta}{2\pi} - \pi r^2 \frac{\Delta\theta}{2\pi} \tag{7}$$

The height of the product at θ degree position $H(\theta)$ is calculated as:

$$H(\theta) = \frac{V_{ABC} - V_A}{S_B} \tag{8}$$

Figure 20 shows the product heights with different blank diameters when $\lambda=0$ in conventional spinning. Figures 21 and 22 show the circumferential distributions of the product heights when $\lambda>0$ in synchronous spinning and conventional spinning, respectively. The heights of the product wall are estimated well when

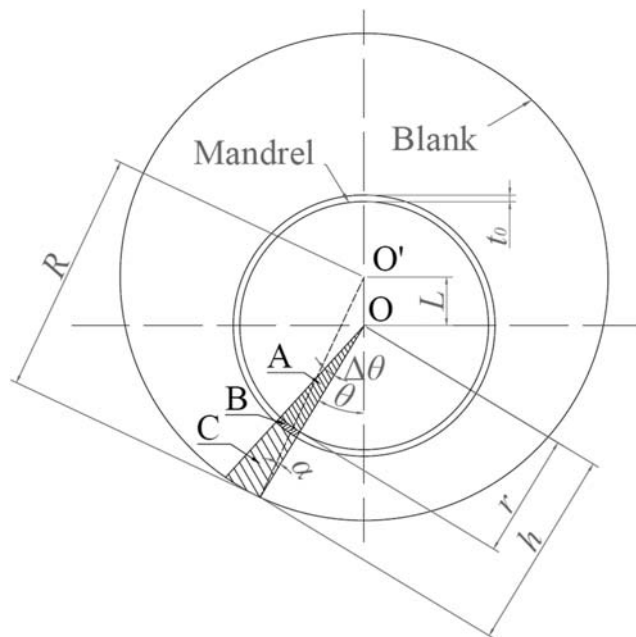


Fig. 19 Estimation of product height

$\lambda=0$ in conventional spinning. When $\lambda>0$, in synchronous spinning, the short side (0°) of the wall is longer than the estimated value, and the long side (180°) of the wall is shorter than the estimated value. The larger the λ , the larger the variation of the roller feed ratio, which causes a larger deviation. When $\lambda>0$, in conventional spinning, the product heights near the long side (180°) of the wall can be estimated well. The product heights near the short side (0°) are still larger than the estimated value with a slight deviation which is smaller than that in synchronous spinning.

5 Forming limit

The forming limits in both synchronous spinning and conventional spinning were investigated in terms of roller feed ratio f , blank diameter D , offset value λ , blank thickness t_0 , and the number of passes. Wrinkling and fracture are observed during the experiments. Wrinkling occurs near the long side of the products at the beginning of the process due to high compressive circumferential stresses [1]. Slight wrinkles were observed in the process and smoothed out in the final product

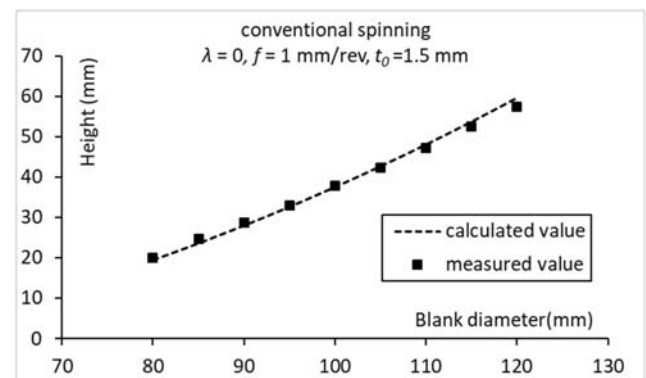


Fig. 20 Product heights with different diameters

Fig. 21 Circumferential distributions of product heights in synchronous spinning

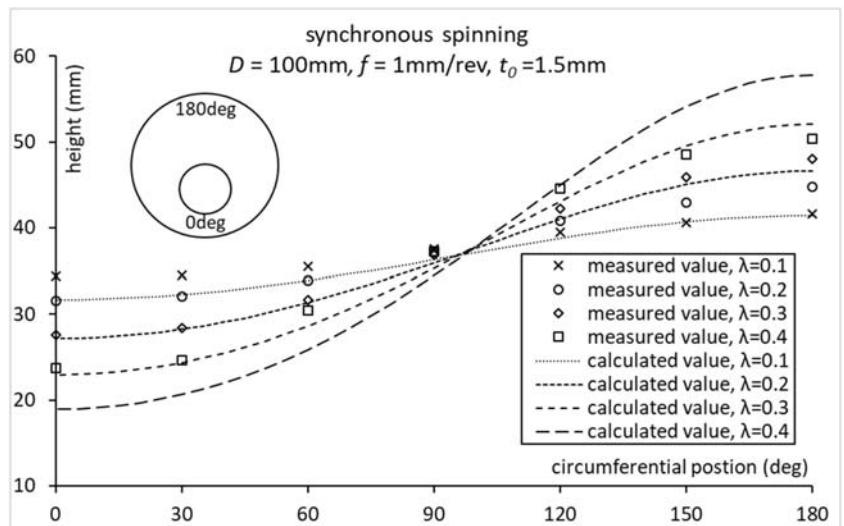


Fig. 22 Circumferential distributions of product heights in conventional spinning

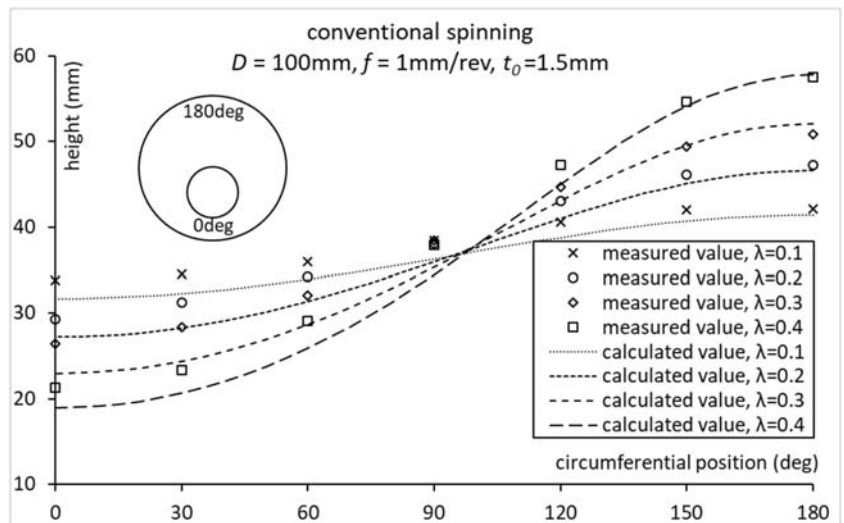


Fig. 23 Wrinkles: **a** synchronous spinning, D 100 mm, λ 0.3, f 1 mm/rev, t_0 1.2 mm, and number of passes 14 and **b** synchronous spinning, D 100 mm, λ 0.5, f 1 mm/rev, t_0 1.2 mm, and number of passes 28

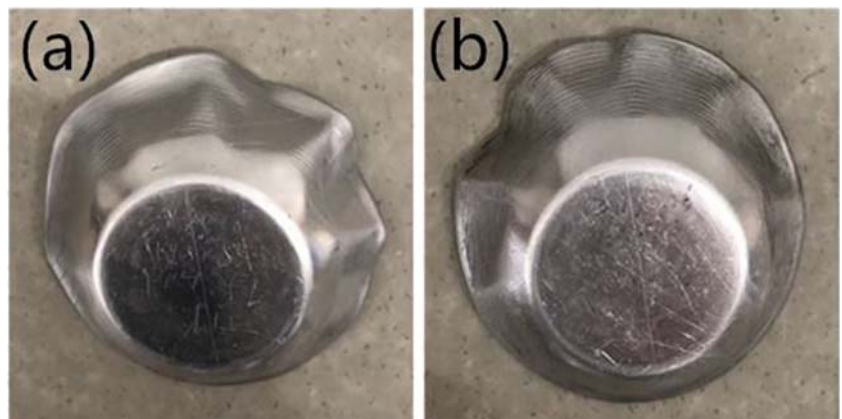
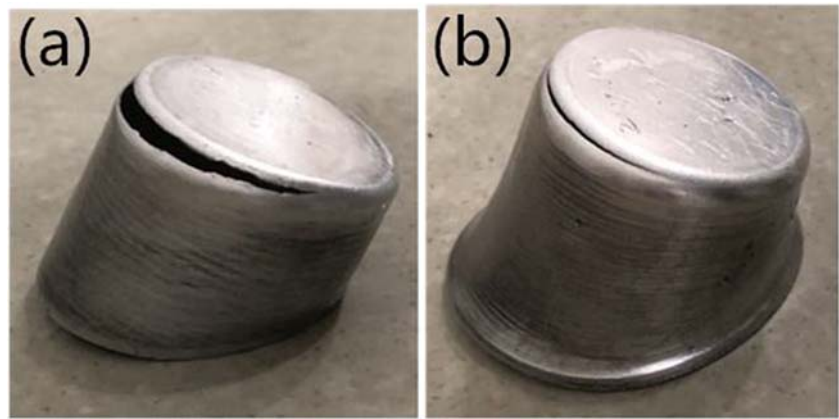


Fig. 24 Fractures: **a** synchronous spinning, D 100 mm, λ 0.3, f 2 mm/rev, t_0 1.5 mm, and number of passes 28 and **b** synchronous spinning, D 110 mm, λ 0.3, f 1 mm/rev, t_0 1.5 mm, and number of passes 14



when $t_0 = 1.2$ mm or blank diameter $D = 120$ mm. Circumferential fractures that are caused by the high tensile radial stress [1] occur at the end of the process near the top of the products. The roller kept colliding into the edge of the product in conventional spinning when $\lambda > 0$, yet, it does not have an obvious effect on the results. Figures 23 and 24 show examples of failed products.

5.1 Offset ratio and roller feed ratio

The forming limit in terms of offset ratio λ and roller feed ratio f was investigated. The parameters are shown in Table 2.

Figure 25 shows the forming limit with blanks of $t_0 = 1.5$ mm in synchronous spinning. Fractures and wrinkles were observed during the experiments. The experiments tend to succeed with a small f and a small λ . Fractures occur as the values of f and λ grow. When f and λ are large enough, wrinkling occurs at the beginning of the process. Wrinkles were more likely to occur when a thinner blank ($t_0 = 1.2$ mm) is used as shown in Fig. 26. The roller feed ratio can be up to 2 mm/rev only when $\lambda = 0$. With a larger λ , the larger feed ratio and a larger flange on the long side of the wall make wrinkling easier to occur. No fracture appeared due to the early wrinkling.

Figure 27 shows the forming limit with blanks of $t_0 = 1.5$ mm in conventional spinning. The forming limit is

Table 2 Parameters of the experiment for forming limit in terms of f and λ

Roller feed ratio f (mm/rev)	1, 2, 3, 4
Blank diameter D (mm)	100
Offset ratio λ	0, 0.1, 0.2, 0.3, 0.4
Blank thickness t_0 (mm)	1.2, 1.5
Number of passes	28

similar to synchronous spinning. The uniform feed ratio in conventional spinning leads to a slightly better result. The experiment succeeded in conventional spinning and failed in synchronous spinning when $\lambda = 0.3$ and $f = 2$ mm/rev. When $t_0 = 1.2$ mm, the forming limit is the same as the one in synchronous spinning as shown in Fig. 28. The uniform feed ratio did not give a better performance which indicates that a large flange contributes more to wrinkling than the roller feed ratio in this case.

5.2 Offset values and blank diameters

The forming limit in terms of offset ratio λ and blank diameter D was investigated. The parameters are shown in Table 3.

Figures 29 and 30 show the forming limit in synchronous spinning when the number of passes is 28 and 14, respectively. Fracture is more likely to occur as D and λ increase. A bigger f or D requires larger spinning forces [1] which makes the workpiece easier to crack. A larger λ means more material on the long side of the product which is equivalent to a larger

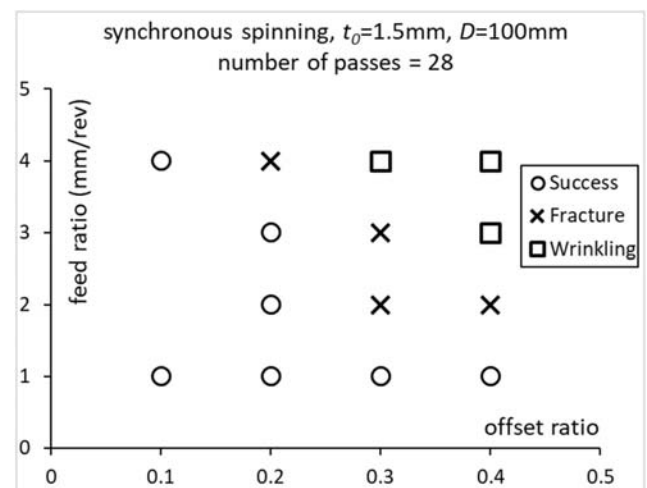


Fig. 25 Forming limit in synchronous spinning when $t_0 = 1.5$ mm

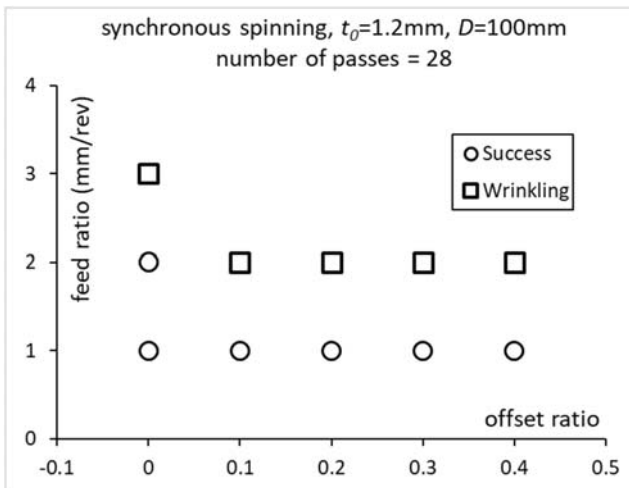


Fig. 26 Forming limit in synchronous spinning when $t_0 = 1.2 \text{ mm}$

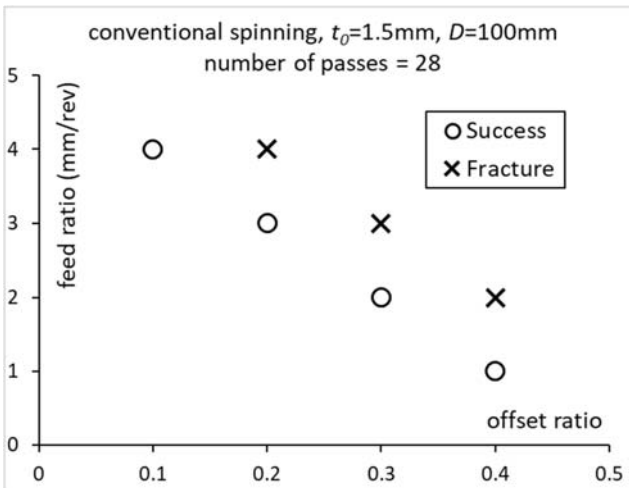


Fig. 27 Forming limit in conventional spinning when $t_0 = 1.5 \text{ mm}$

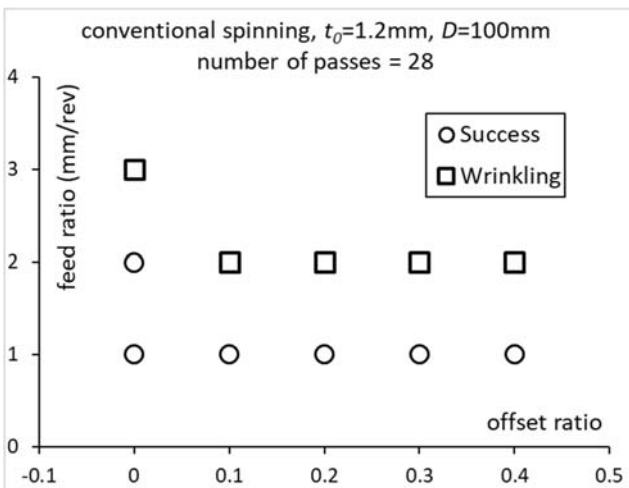


Fig. 28 Forming limit in conventional spinning when $t_0 = 1.2 \text{ mm}$

Table 3 Parameters of the experiment for forming limit in terms of f and D

Roller feed ratio f (mm/rev)	1
Blank diameter D (mm)	90, 100, 110, 120
Offset ratio λ	0, 0.1, 0.2, 0.3, 0.4, 0.5, 0.6, 0.7, 0.8
Blank thickness t_0 (mm)	1.2, 1.5
Number of passes	14, 28

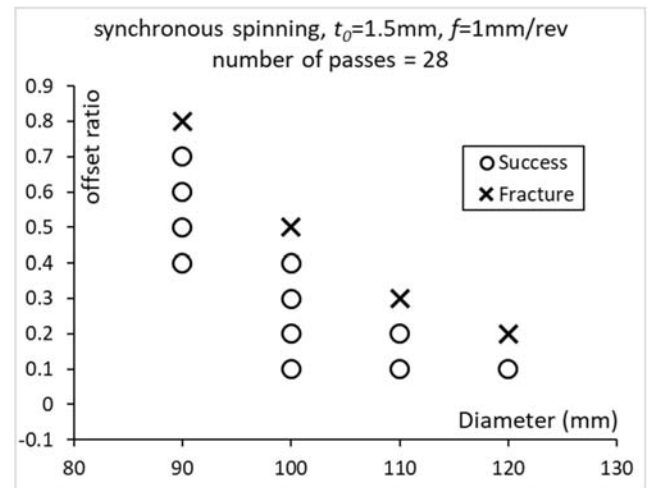


Fig. 29 Forming limit in synchronous spinning when $t_0 = 1.5 \text{ mm}$ and the number of passes is 28

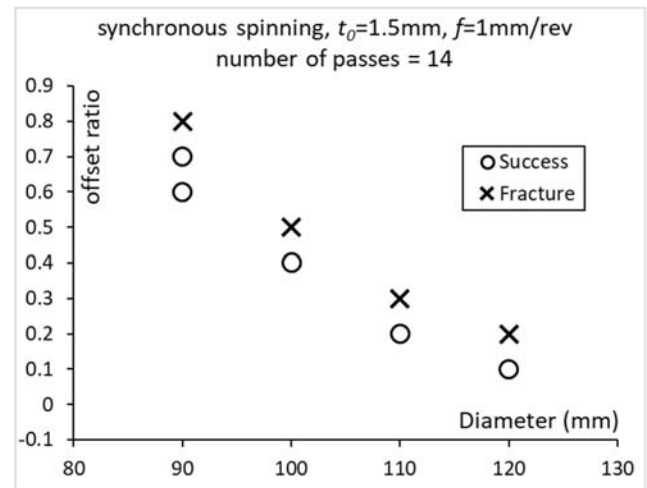


Fig. 30 Forming limit in synchronous spinning when $t_0 = 1.5 \text{ mm}$ and the number of passes is 14

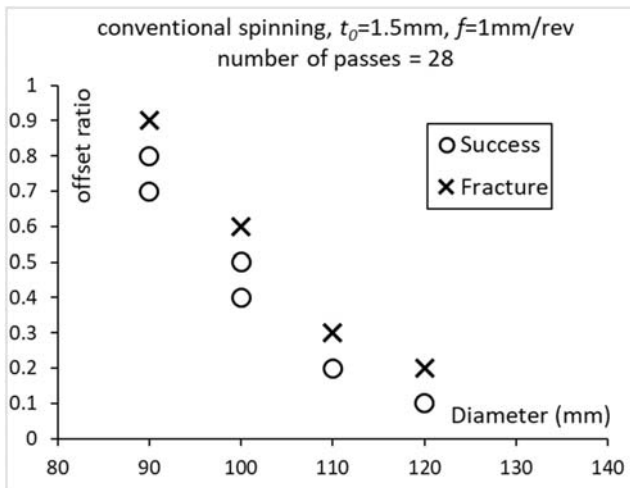


Fig. 31 Forming limit in conventional spinning when $t_0 = 1.5$ mm and the number of passes is 28

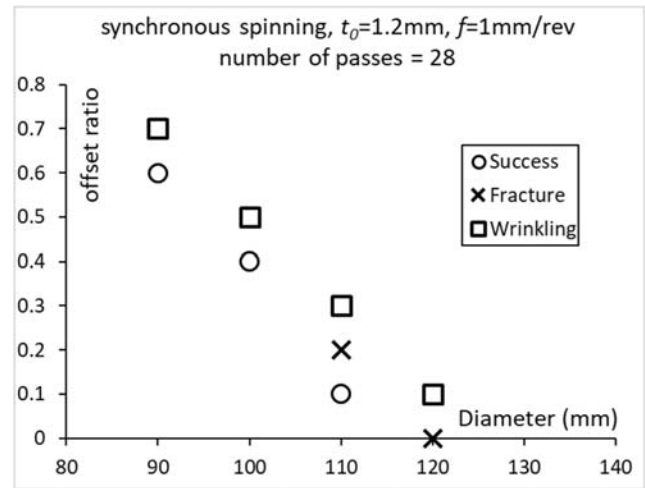


Fig. 33 Forming limit in synchronous spinning when $t_0 = 1.2$ mm and the number of passes is 28

D , and it also results in a larger variation of f in synchronous spinning. A smaller number of passes does not affect the forming limit in this case.

Figure 31 shows the forming limit in conventional spinning when the number of passes is 28. The feed ratio on the long side of the wall (180°) is reduced compared with synchronous spinning with the same parameters, which improves the forming limits when $D = 90$ mm and 100 mm. However, the feed ratio did not affect the forming limits due to larger flanges when $D = 110$ mm and 120 mm.

The material built up in front of the roller in the backward pass and was pushed out of the wall on the short side of the products when $\lambda > 0.6$ and blank diameter is $D = 90$ mm as shown in Fig. 32. This phenomenon is reduced when the number of passes is small or a smaller λ is used.

Figure 33 shows the forming limit when $t_0 = 1.2$ mm, and the number of passes is 28 in synchronous spinning. Compared with $t_0 = 1.5$ mm, wrinkles are more likely to occur when $t_0 = 1.2$ mm. Wrinkles tend to occur as λ or D increases. When $D = 90$ mm and 100 mm, the products are fracture-free

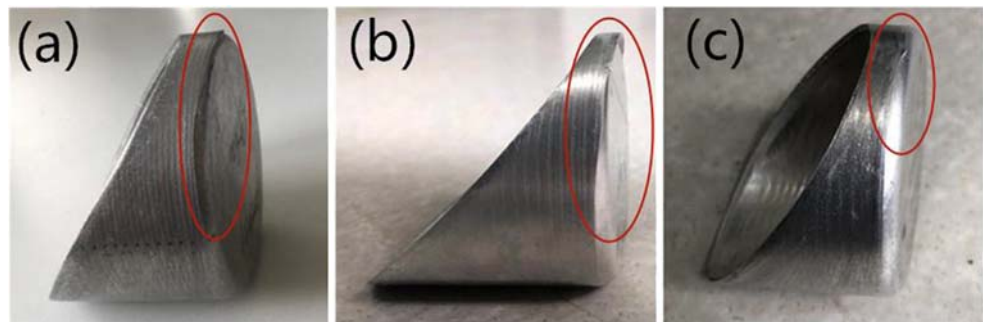
due to the small flange. When D is large, fractures tend to occur before wrinkles as λ increases. Figure 34 shows the forming limit when $t_0 = 1.2$ mm, and the number of passes is 14 in synchronous spinning. The number of passes affects the forming limit when a small t_0 is used. Wrinkling is easier to occur with a smaller number of passes. No fractures were observed in this case.

6 Conclusion

In this study, two kinds of spinning methods for offset blank are conducted. The conclusions are as follows:

1. The axial distribution of wall thickness at 90° position of the product when $\lambda > 0$ nearly coincides with that when $\lambda = 0$. The thickness increases circumferentially from the lower side to the higher side of the wall when $\lambda > 0$.
2. The bigger the λ , the greater the difference of the thickness distribution on the short side and the long side of the wall.

Fig. 32 Excessive material flow on the short side of the wall: **a** synchronous spinning, D 90 mm, λ 0.7, and number of passes 28; **b** conventional spinning, D 90 mm, λ 0.8, and number of passes 28; and **c** synchronous spinning, D 90 mm, λ 0.7, and number of passes 14



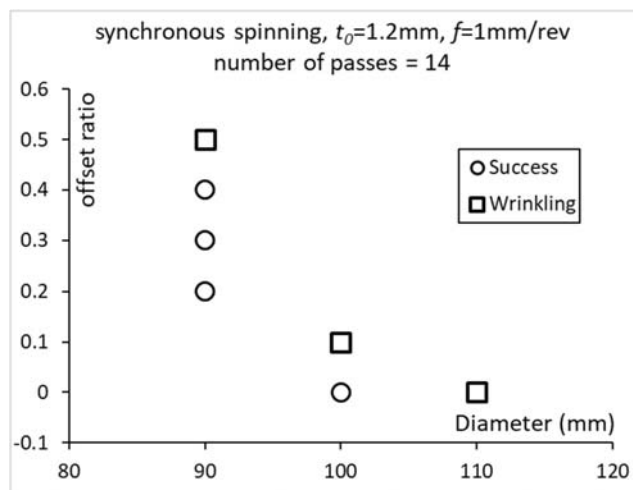


Fig. 34 Forming limit in synchronous spinning when $t_0 = 1.2$ mm and the number of passes is 14

- Due to the uniform feed ratio, the difference of the distribution of the wall thickness on the product formed in conventional spinning is smaller compared with that in synchronous spinning.
- The wall height of the product can be well estimated when $\lambda = 0$. In synchronous spinning, the larger the λ , the larger the deviation between the measured height and the estimation. In conventional spinning, the product heights near the long side (180°) of the wall can be estimated well; the product heights near the short side (0°) is still larger than the estimated value with a slightly smaller deviation than that in synchronous spinning.
- Wrinkling tends to occur as λ and f increase when a small t_0 is used. Fracture tends to occur as λ and f increase when a large t_0 is used.
- The number of passes has a larger effect on the forming limit when a smaller t_0 is used.
- Conventional spinning has a better performance on producing asymmetric shapes with offset blanks than synchronous spinning.

Funding information This work was financially supported by the Chinese Aeronautical Establishment [2018ZE54028] and Natural Science Foundation of Liaoning Province, China [2019ZD0240].

References

- Music O, Allwood JM, Kawai K (2010) A review of the mechanics of metal spinning. *J Mater Process Technol* 210:3–23
- Amano T, Tamura K (1984) The study of an elliptical cone spinning by the trial equipment. In: Proceedings of the 3rd international conference on rotary metalworking processes. Kyoto, Japan, pp 213–224
- Gao XC, Kang DC, Meng XF, Wu HJ (1999) Experimental research on a new technology—ellipse spinning. *J Mater Process Technol* 94(2–3):197–200
- Xia QX (2003) The spinning formed technology and machine of the 3D non-axisymmetric parts. *New Technol New Process* 12:33–35 (In Chinese)
- Xia QX, Xie SW, Huo YL, Ruan F (2008) Numerical simulation and experimental research on the multi-pass neck-spinning of non-axisymmetric offset tube. *J Mater Process Technol* 206(1–3):500–508
- Xia QX, Cheng X, Long H, Ruan F (2012) Finite element analysis and experimental investigation on deformation mechanism of non-axisymmetric tube spinning. *Int J Adv Manuf Technol* 59(1–4):263–272
- Xia QX, Lai ZY, Zhan XX, Cheng XQ (2010) Research on spinning method of hollow part with triangle arc-type cross section based on profiling driving. *Steel Res Int (Spec Ed)* 81(9):994–997
- Awiszus B, Meyer F (2005) Metal spinning of non-circular hollow parts. In: Proceedings of 8th ICTP. Verona, Italy, pp 353–355
- Arai H (2005) Robotic metal spinning—forming asymmetric products using force control. In: Proceedings of 2005 IEEE international conference on robotics and automation. Barcelona, Spain, pp 2702–2707
- Arai H (2006) Force-controlled metal spinning machine using linear motors. In: Proceedings of the 2006 IEEE international conference on robotics and automation. Orlando, Florida, pp 4031–4036
- Shimizu I (2010) Asymmetric forming of aluminum sheets by synchronous spinning. *J Mater Process Technol* 210:585–592
- Han ZR, Xu Q, Jia Z, Li XB (2015) Experimental research on oblique cone die-less shear spinning. *Proc Inst Mech Eng B J Eng Manuf* 78(23):11772–11782
- Jia Z, Han ZR, Liu BM, Fan ZJ (2017) Numerical simulation and experimental study on the non-axisymmetric die-less shear spinning. *Int J Adv Manuf Technol* 92:497–504
- Jia Z, Han ZR, Xu Q (2015) Effects of processing parameters on the surface quality of square section die-less spinning. *Int J Adv Manuf Technol* 80:1689–1700
- Jia Z, Han ZR, Xu Q, Peng WF (2014) Numerical simulation and experiment study on hollow spinning process for square cross-section cone. *Int J Adv Manuf Technol* 75:1605–1612
- Härtel S, Laue R (2016) An optimization approach in non-circular spinning. *J Mater Process Technol* 229:417–430
- Sekiguchi A, Arai H (2012) Control of wall thickness distribution by oblique shear spinning methods. *J Mater Process Technol* 212(4):786–793
- Han ZR, Fan ZJ, Xiao Y, Jia Z (2016) A research on thickness distribution of oblique cone in dieless shear spinning. *Int J Adv Manuf Technol* 90:2901–2912
- Sugita Y, Arai H (2015) Formability in synchronous multipass spinning using simple pass set. *J Mater Process Technol* 217:336–344
- Arai H, Kanazawa T (2018) Synchronous multipass spinning of oblique-bottom shape. *J Mater Process Technol* 260:66–76
- Xiao Y, Han ZR, Fan ZJ, Jia Z (2018) A study of asymmetric multipass spinning for angled-flange cylinder. *J Mater Process Technol* 256:202–215
- Wang L, Long H, Ashley D, Roberts M, White P (2011) Effects of roller feed ratio on wrinkling failure in conventional spinning of a cylindrical cup. *Proc Inst Mech Eng B J Eng Manuf* 225:1991–2006
- Essa K, Hartley P (2010) Optimization of conventional spinning process parameters by means of numerical simulation and statistical analysis. *Proc Inst Mech Eng B J Eng Manuf* 224:1691–1705

Publisher's note Springer Nature remains neutral with regard to jurisdictional claims in published maps and institutional affiliations.